FULL-SCALE LABORATORY TESTING OF A GEOSYNTHETICALLY REINFORCED SOIL RAILWAY STRUCTURE

A.F. Esen[1], P.K. Woodward[2], O. Laghrouche[1], T. M. Čebašek[2], A.J. Brennan[3], S. Robinson[3], D.P. Connolly[2]

[1]Institute for Infrastructure and Environment, Heriot-Watt University, Edinburgh EH14 4AS, UK

[2]Institute for High-Speed Rail and System Integration, University of Leeds, Leeds LS2 9JT, UK

[3]School of Science and Engineering, University of Dundee, Dundee DD1 4HN, UK

Abstract

Railway lines typically use traditional sloping embankments as the principal means of track support. However, the use of Geosynthetically Reinforced Soil (GRS) systems have gained popularity as alternatives to conventional embankments, particularly for high-speed lines in Japan. This system requires less ground stabilization/improvement and less land take than conventional embankments due to its smaller base area. This research investigates the immediate and long-term settlement behaviour of a Geosynthetically Reinforced Soil with Retaining Wall (GRS-RW) system subject to cyclic loading for two track forms: a concrete slab track and a ballasted track. First, a three-sleeper concrete slab section is constructed at full-scale under controlled laboratory conditions, followed by a ballasted track. Both are supported on a 1.2m deep subgrade and a frost protection layer in accordance with railway design standards. Two different axle load magnitudes are applied statically, and then cyclically/dynamically, using 6 actuators to replicate moving train axle loads. It is observed that the slab track performs significantly better in terms of elastic and plastic deformation under both static and cyclic loading. Overall, the amplitude of the rail displacement under an individual cycle loading was approximately 25% lower for the slab track and the amplitude of the sleeper displacement on the ballasted track was approximately 6-7 times higher.

Keywords: *Full-scale cyclic loading; Railway track settlement; Geosynthetically Reinforced Soil; Long-term rail track behaviour; Ballast and concrete slab track; Railway Embankment*

1 Introduction

The growing demand for rail lines leads railway infrastructure companies to trim the life-cycle costs of railways due to increasing economic pressures. This is particularly true for high-speed lines but equally applicable to conventional-speed lines. In addition to the ongoing discussion on the performance of the ballasted and the ballastless (slab) tracks, alternative types of track support structures are also being proposed to improve the inherent track quality while lowering the upfront capital construction costs.

Geogrids are proven to be a practical solution used under the ballast to reduce the permanent deformation for railways (Yu, et al., 2019; Singh, et al., 2020; Punetha, et al., 2020). In the last

decades, geosynthetically reinforced soils (GRS) emerged as a reliable transportation infrastructure mitigation strategy. GRS structures have been constructed extensively at various infrastructures along highways, particularly at bridge abutments all over the world (Lee & Wu, 2004; Lenart, et al., 2016; Berg, et al., 2009; Wu, 2018; Herold, 2005; Helwany, et al., 2003; Skinner & Rowe, 2005; Kim & Kim, 2016). Embankments have been used as the principal means of supporting the railway track for nearly 200 years (Connolly, et al., 2013). Indeed, modern high-speed railway lines still typically use traditional sloping embankments for track support over flood plains and for route and track geometry considerations (e.g. China and Europe) (Connolly, et al., 2014). However, in Japan, the application of geosynthetically reinforced soil substructures in combination with retaining walls (GRS-RW) have gained popularity as alternatives to conventional embankments, particularly for high-speed lines like the Hokkaido Shinkansen, which is an extension from the high-speed lines from Tokyo (Yonezawa, et al., 2014). A construction system of geosynthetic-reinforced soil (GRS) with full height rigid (FHR) facing retaining walls (RWs) is now widely used in Japan. The total length was more than 180km in 2018 (Tatsuoka, 2019).

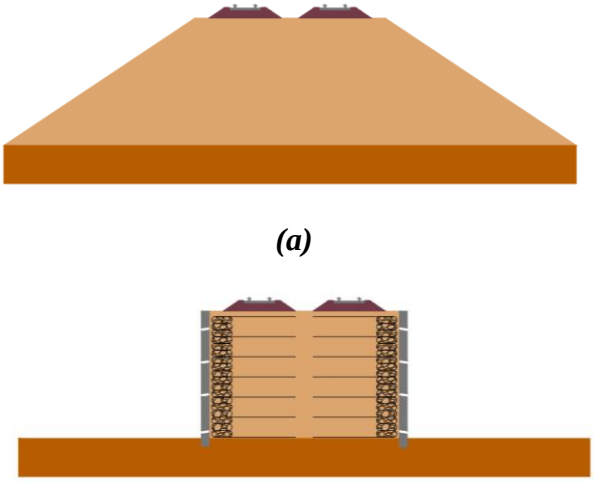

(a)

(b)

Figure 1: Land occupation of; ***(a)*** a conventional embankment, and ***(b)*** GRS-RW system

These structures provide cost-effective solutions since they require less ground stabilization/improvement (Dong, et al., 2018) and land take than conventional embankments with a much smaller base area (**Figure 1**). They also provide lower residual displacements during operation, i.e. better operational performance than conventional embankments. A large number of field investigations have been conducted to provide design methodology for materials, and construction steps to build a GRS-RW structure for high-speed railways (Horii, et al., 1994; Koseki, et al., 1996; Tatsuoka, et al., 1997; Koseki, et al., 2006; Tatsuoka, et al., 2007; Koseki, 2012; Tatsuoka, et al., 2014; Yonezawa, et al., 2014; Tatsuoka, 2019; Tatsuoka & Watanabe, 2015). Overall, structural stability is provided by the retaining walls, backfill and the geosynthetics wrapped around gravel bags located directly behind the retaining walls. In addition, reinforced-soil walls are generally more flexible than conventional retaining

structures. Thus, they may be used in areas where large uneven displacements are expected due to surface movements during earthquake events.

The GRS-RW also takes advantage of full-height-rigid facing (FHR) which allows better control over concentrated loads – an area that is particularly beneficial in railway applications. Typical reinforced wall structures that use discrete wall panels can suffer severe damage if there is a loss of stability of one of the panels. This, obviously, causes significant concerns and issues for railways. The minimum specified FHR facing concrete thickness for GRS-RW is 30cm, which is based on constructability considerations. The facing is therefore very thin and the required amount of steel-reinforcement in the facing is minimal. This thickness is typically larger than that based on structural requirements. The maximum height of a GRS retaining wall (with FHR facing) is recorded as 11m, while the tallest GRS bridge abutment is 13.4m high (Tatsuoka, et al., 2014). Care needs to be taken at low wall heights to prevent a lack of confining pressure causing active stability issues, hence the use of the gravel bags to provide lateral support during construction.

The basic advantage of the GRS-RW system, over a conventional cantilever structure with unreinforced soil backfill, is in obviating the need to provide a piled foundation to resist the lateral thrust developed due to active earth pressure conditions, the large internal moments, and shear forces developed in the facing. This is particularly the case when constructing over soft soils and when high wall heights are considered. Removing piles reduces costs dramatically and makes the structure more resilient to seismic events where large ground movements may occur. The base ground for existing *in-situ* GRS-RW walls was improved by using 1m deep cement-mixed soil with a cement content of 150kg per cubic meter, and above that, a drainage layer consisting of crushed gravel was placed (Tatsuoka, et al., 2007). The degree of compaction applied to the backfill, and the induced tensile stresses in the geosynthetic reinforcement are critical elements of the construction technique to ensure a successful installation, i.e. to significantly reduce lateral pressure on the facing. Pre-loaded and pre-stressed gravel backfill for GRS-RWs with full-height rigid facing has also been implemented in practice for a railway line in Kyushu Island, Japan. Its high seismic stability capability was confirmed through model shaking tests (Koseki, 2012).

A strong connection between the facing and the backfill is essential for a stable GRS-RW structure. The gravel-filled bags placed at the wall face have a very high drainage capacity and thus any excess pore pressure generated in the backfill during loading can efficiently dissipate to leave a drained condition (**Figure 1b**). Furthermore, some of the facing concrete penetrates the surface zone of the gravel-filled bags during placement and therefore increases the contact strength between the concrete facing and the bags.

In order to investigate the performance of railway track structures under static and cyclic loading, full-scale laboratory testing has been used by many researchers (Čebašek, et al., 2018; Woodward, et al., 2014; Bian, et al., 2014; Brown, et al., 2007; Yu, et al., 2019). With the help of this useful approach, short- and long-term behaviour of railway track components have been investigated. As a consequence of cumulative deformation under repeated loading, various settlement models have been proposed (Alva-Hurtado & Selig, 1981; Shenton, 1985; Sato,

1995; Bian, et al., 2014; Selig & Waters, 1994; Thom & Oakley, 2006; Indraratna, et al., 2012). Comparisons between experimental and analytical models have been performed by Dahlberg (2001) and Abadi et al. (2016), highlighting two phases of settlement which consist of a non-linear relationship between the number of cycles and initial settlement followed by a linear trend. Čebašek et al. (2018) compared the performance of ballasted track against slab track on conventional embankment. Their results demonstrated that settlement of the concrete-slab track is significantly lower than that of ballasted track under similar loading and ground conditions.

This research work seeks to provide a technical insight of an adoption of the GRS-RW system for both developing and developed countries which are set to expand high-speed rail infrastructures rapidly while increasing the track performance and reducing the construction costs. In this study, the purpose is to compare a concrete-slab and ballasted tracks on GRS embankment. Short and long term behaviour are investigated using a full-scale testing facility called Geo-pavement and Railways Accelerated Fatigue Testing (GRAFT-2). The superstructures are positioned over a geosynthetically reinforced soil with retaining wall (GRS-RW) system and subjected to static and cyclic loading. The testing facility, construction of the structure, track components and material parameters are all described in Section 2 of the paper. The loading methodology and data acquisition are presented in Section 3 and the analysis of the results are discussed in Section 4, followed by the Conclusions of the testing programme.

2 Laboratory testing

In this section, the methodology of the tests, experimental setup, materials and their associated properties are described.

2.1 Methodology

A GRS-RW system was investigated in controlled laboratory conditions using GRAFT-2 facility (**Figure 2**), located at Heriot-Watt University. The accelerated testing approach means multiple axle passages can be simulated in a short time period. This was achieved using six independent hydraulic actuators loading three full-sized sleepers on a ballasted track or on a concrete slab track via built-in baseplate locations on the concrete surface. This simulated the passage of a moving axle (using phased loading), with each piston applying loads on a given rail segment as indicated in **Figure 4**. The primary objective of testing was to assess and characterise the short- and long-term settlement behaviour of a GRS-RW structure subjected to cyclic loading using the two different track forms. Firstly, the concrete slab track was tested followed by the ballasted track. The results presented in this paper were performed on a GRS-RW system in accordance with railway infrastructure standards. A similar testing procedure was followed by Čebašek et al. (2018) in earlier GRAFT-2 testing of ballasted and concrete slab-track, thus allowing for comparisons to be made with non-GRS-RW support structures in future work.

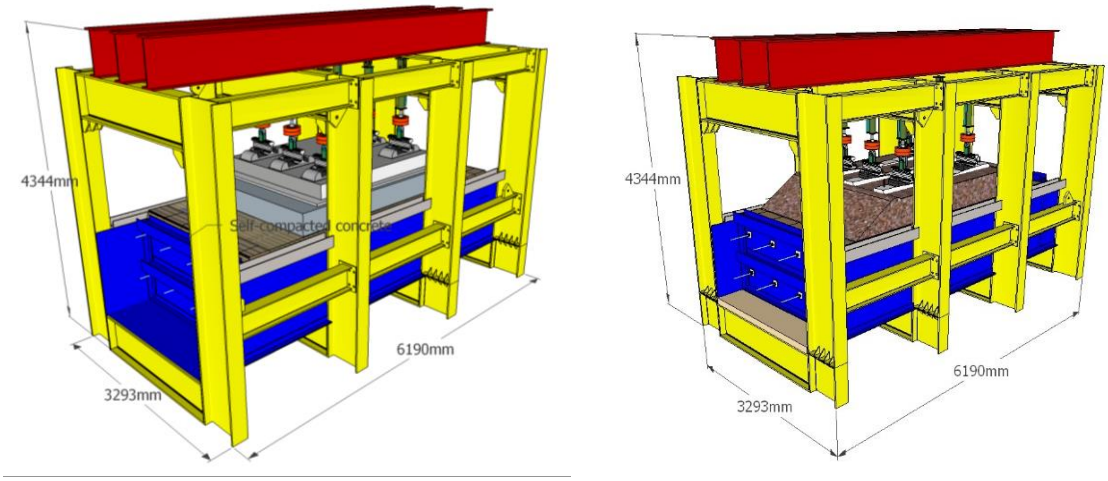

(a) ***(b)***

Figure 2: *Geopavement and Railways Accelerated Testing Facility (GRAFT-2) at Heriot-Watt University,* ***(a)*** *slab track and* ***(b)*** *ballasted track resting on GRS-RW structure*

2.2 Experimental setup

The GRAFT-2 facility was used to test sections of a precast concrete slab track, and a ballasted track with concrete sleepers. The substructure consisted of 0.1m well-compacted base layer on top of which the 1.2 m high GRS-RW was built. The substructure layers are the subgrade and frost protection layer (FPL) from bottom to top, respectively. The sand mixture was chosen from two different batches composed of 0-6mm well-graded granular limestone **Figure 9**. The sand was comprised of 80% of 0-4mm batch and 20% of 2-6mm batch. This was adopted to be consistent with the conventional embankment testing (Čebašek, et al., 2018), and also to be consistent with HS line design where the second deformation modulus (EV_2) is 120MPa. The general concept of the GRS-RW structure for the two track types tested in the GRAFT-2 facility is presented in **Figure 3**.

The fill consisted of geogrid reinforced layers with symmetrically embedded bolts at selected positions. Tensar RE540 is a uniaxial geogrid made of high-density polyethylene with enhanced long-term tensile strength. The properties of the geogrids used in this study are given in **Table 1**.

Table 1: *Properties of geogrids used in soil and ballast*

RE540	**TX190L**
Plan view	

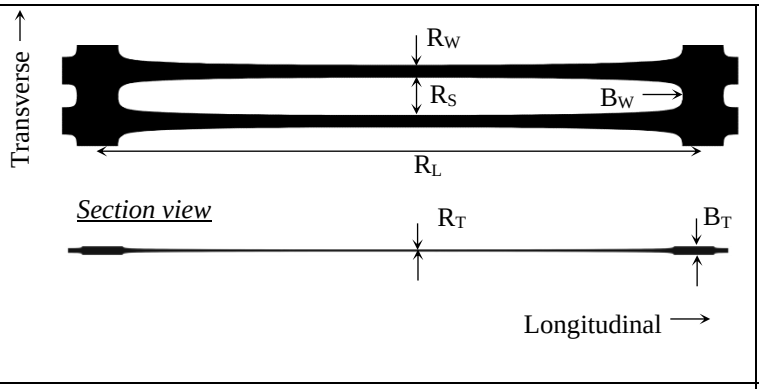

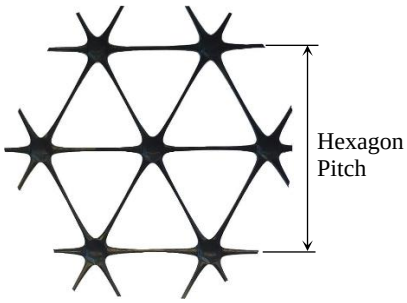

Uniaxial		Triaxial	
Used for soil reinforcement		Used under ballast	
R_L (mm)	235	Aperture shape	Triangular
R_S (mm)	16	Rib shape	Rectangular
R_W (mm)	6	Hexagon pitch (mm)	60
R_T (mm)	1.1		
B_T (mm)	2.5-2.7	Junction efficiency (%)	100
B_W (mm)	16		
Mean Aperture size	16 x 219	Mean Radial Secant Stiffness at 0.5% Strain (kN/m)	540
Short term tensile strength in longitudinal direction (kN/m)	64.5		
Junction efficiency (%)	95		

The geogrid was placed over the base layer then the gravel bags were positioned at the ends; the overlapping gravel bags were placed in a similar fashion to that of a brick wall construction at the shoulders (**Figure 3a**). A sand fill layer was then formed by compacting sand (**Figure 3b**). The geogrid was then pulled and tightened over the gravel bags and pinned into the compacted soil using nails to provide tensile strength (**Figure 3c**). The geogrid was partially wrapped and hand-tightened to improve the overall stiffness of the reinforced soil. Subsequent layers were constructed sequentially up to a total wall height of 1.2m. During this construction process steel tie bars were positioned between the layers, as shown in **Figure 4** (the free-standing retaining wall is represented by the blue steel plates).

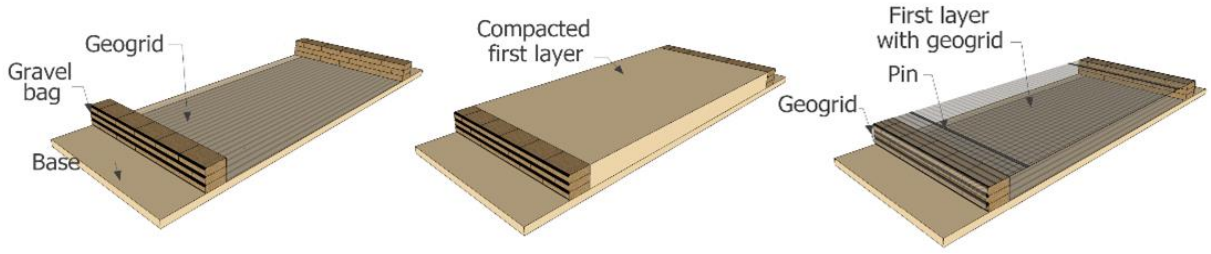

(a) ***(b)*** ***(c)***

Figure 3: *The stages of the GRS-RW construction*

The steel tie bars were anchored within the fill subgrade by embedded steel *angle-sections* (**Figure 4a**). The steel plates were used to replicate the *in-situ* formed GRS-RW system

retaining wall and were only connected to the steel bars once the full subgrade structure had been formed. The gaps between the steel plate and the gravel bags were then filled with self-compacting concrete to form a fully connected wall retaining system.

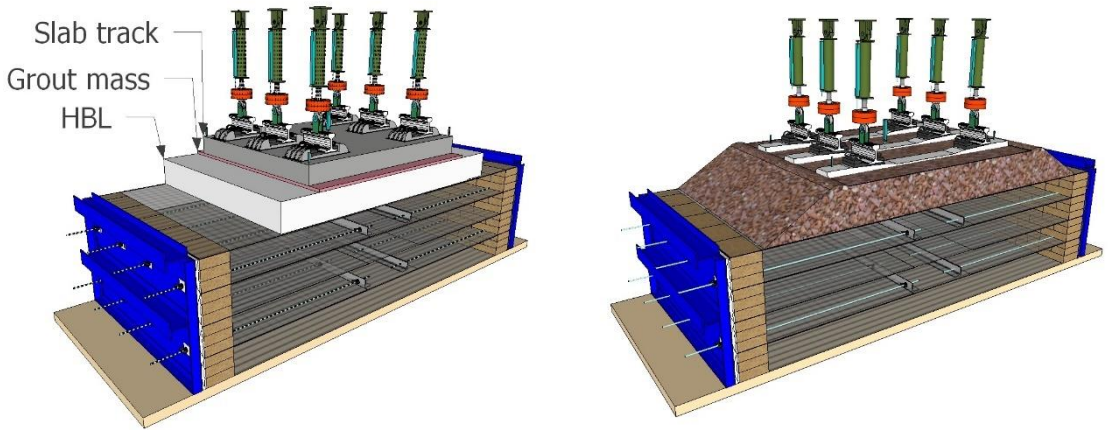

(a) ***(b)***

Figure 4: *Layout of the ballast and slab tracks on GRS-RW embankment (a) concrete slab-track; (b) ballasted track*

The gravel bags played an important role during construction as temporary (and stable) facings, resisting lateral earth pressure generated by the backfill compaction stresses and the self-weight of the structure. For the real *in-situ* structure the gravel bags facilitate the compaction of the layer during construction and create a barrier of differential horizontal and vertical displacement between the GRS structure and the wall. They also serve as a drainage route.

Table 2: *CBR values of the compacted soil using Dynamic Cone Penetrometer (DCP)*

CBR Test Time	**CBR value**
During construction of Substructure -Subgrade	28.5
During construction of Substructure -FPL	56.1
After Removal of Slab - on top of FPL	125.1
After Removal of Ballast – on top of FPL	128.2

The compaction level of each 0.3m high layer was set based on a correlation with CBR values, which were obtained via measured Dynamic Cone Penetrometer (DCP) tests as shown in **Table 2**. The correct compaction level was essential in order to achieve the required stiffness. The indicated CBR values have been identified in conjunction with the work carried out by Čebašek, et al. (2018) who made a correlation between the EV_2 and CBR.

2.2.1 Laboratory construction of substructure

Photographs of the construction stages of the substructure are highlighted in **Figure 5** and **Figure 6**. The geogrid was cut 11m long and placed on each base layer. The substructure test bed width was 5m. To cover the 2.2m width of the test bed the geogrids were placed as 2 pieces

of 1.2m and 1.0m widths. They were placed in such a way that at each layer the connections of two pieces of geogrid did not overlap each other. The joint was staggered as the geogrid layers were placed during the GRS construction. Three layers of sandbags were placed at opposite ends of the test bed (5m apart) and compacted using hand tools (**Figure 5a**). Then the well-graded sand was placed between sand bag walls and compacted with a forward/reverse plate compactor (**Figure 5b)**. The initial loose sand thickness was 200mm which reduced to 150mm after compaction. The two compacted layers formed a 300mm thick total compacted layer which had the same thickness as the compacted sand bag walls. The sand level was checked using a conventional spirit level. Once the sand bag walls and compacted sand reached the same height, the geogrid was wrapped around the bags and laid on the compacted sand (**Figure 5c**).

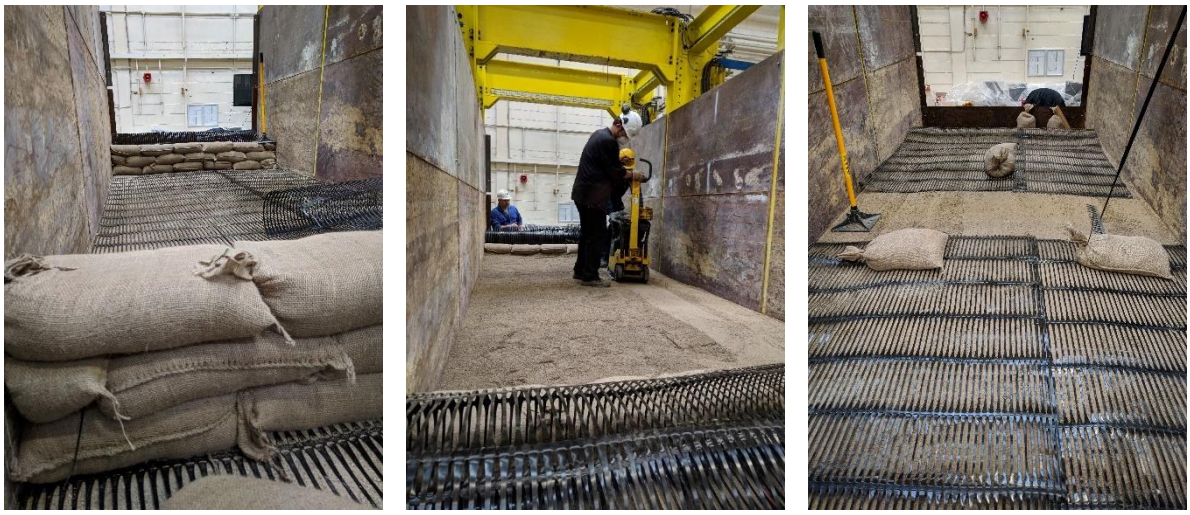

(a) ***(b)*** ***(c)***

Figure 5: *Construction stages of the GRS structure: (a) Positioning the sandbags on the geogrid; (b) compaction of the sand; and (c) wrapping the geogrid around the sandbags and pinned into compacted soil*

The geogrid then was hand-tightened and fixed to the soil using nails. Each layer of reinforced soil was formed following the same soil compaction parameters given in Cebasek et al. (2018). The first 800mm of the subgrade was compacted to achieve an EV_2 value of 60MPa and the remaining upper FPL 400mm was compacted to achieve an EV_2 value of 120MPa. As commented above these elasticity values were calibrated via DCP measurements during each compaction layer formation.

(a) ***(b)*** ***(c)***

Figure 6: *Construction stages of the GRS structure: (a) Tie bars through the sandbags and FHR wall, and anchored with angle irons; (b) Self-standing GRS soil and the cast-in HBL layer of slab track (c) FHR retaining wall positioned with topflow*

At 300mm and 900mm depths tie bars were anchored to angle irons that were positioned half a metre from each other, i.e. in the middle of the 5m track width (**Figure 6a**). The vertical and horizontal distance of each adjacent tie bar was 600mm, which are designed according to Tatsuoka, et al. (1997). In total four layers of reinforced soil were constructed. On top of this substructure, the hydraulically bonded layer (HBL) was placed (**Figure 6b)**.

Finally, the 0.08m gap between the GRS wall and RW was filled with 'topflow' as seen in **Figure 6c**. It was a ready-mix highly fluid self-compacting concrete consisting of maximum 10mm diameter aggregates. This material was chosen specifically because of its ability to fill the gaps between the geogrid and sandbags through geogrid apertures. This was to provide reinforcement and resilience to the GRS. The density, Young's modulus, and Poisson's ratio of the topflow were determined using compression tests on cylindrical samples and found to be 2428,7kg/m3, 21.2GPa and 0.159, respectively.

2.2.2 Concrete slab track

The first form of the superstructure was constructed using a Max Bögl slab track which consists of a prefabricated reinforced concrete slab made of c45/55 concrete with characteristic cube compressive strength of 45 MPa, which is a high strength concrete. As shown in **Figure 7a**, a three-sleeper section was used for the concrete slab-track which was placed above the Hydraulically Bonded Layer (HBL). The HBL itself was of thickness 300 mm and it was made of c10/12 concrete with characteristic cube compressive strength of 10 MPa, which is a lightweight and low strength concrete. After 21 days, the slab was positioned above the HBL supported by hard wooden wedges. Then 'Conbextra HF', a high-flow, non-shrink, cementitious grout, for grouting gap thicknesses between 10 to 100mm, was used between the slab and the HBL.

Figure 7: *Slab track in the GRAFT-2 testing facility*

The rail fastening system was the 300-1 Vossloh Fastening System. From bottom to top the rail support consisted of three layers: an EPDM pad, which is a soft synthetic rubber railpad, a steel baseplate, and an EVA, which is a stiff copolymer pad for rail seating, respectively. The static stiffness of the EPDM was about 22.5kN/mm and the dynamic stiffness was about 40kN/mm. The static stiffness of the EVA pad was about 600–700kN/mm and the dynamic stiffness was about 1600–1800kN/mm. The cut rail segments used in the slab track test were 60E1 (UIC 60).

2.2.3 Ballasted track

After completion of the slab track tests, the superstructure including the HBL, grout and concrete slab were removed from the facility. The surface of the substructure soil required removal as the HBL layer disturbed the upper soil layer. The upper 50mm of sand was therefore excavated and replaced with a new sand layer which was then compacted to achieve the same stiffness as the subgrade prior to the concrete slab track test. A triangle-aperture geogrid TX190L was placed on top of the substructure to provide additional support to the ballast. **Figure 8** shows the position of the sleepers (standard G44s) on the ballast bed at a typical industry spacing of 650mm. The ballast bed was placed and compacted in four equal layers of 100mm intervals and hence its overall thickness underneath the sleepers was 400mm. In order to reach the required ballast compaction, an electric compactor with a 400mm by 320mm vibrating plate was used to compact each 100mm thickness ballasted layer. As a result, the bulk density of the compacted ballast was approximately 16kN/m^3.

Figure 8: *Ballast track in the GRAFT-2 testing facility*

The ballast aggregate was composed of micro-granite at 0.5% moisture content. The plot of **Figure 9** indicates the gradation curve of the ballast which is a good match for a typical railtrack ballast curve, compared to that of the sand curve used to construct the subgrade and FPL. The lower EPDM elastic pads used in the ballast test were the same rail pads as those used in the concrete slab track test. Pandrol's fast clip fastening system was used to restrain the loaded rail segments to the sleepers. Sections of BS113A (56E1) rail segments were used in the ballasted track test. The purpose of the rail segments use was to allow the connection of the actuators to the sleepers. As these were separate rail segments, they did not contribute to the bending stiffness of the track in the experiments and thus they did not have any effect on the track deformation. The rail segments' role is to be the connectors between the track and the actuators. *Note: this is often normal practice in the laboratory testing of railway track*. More than 3 million load cycles were applied in this ballasted-track test following the same procedure as that applied in the concrete slab track tests.

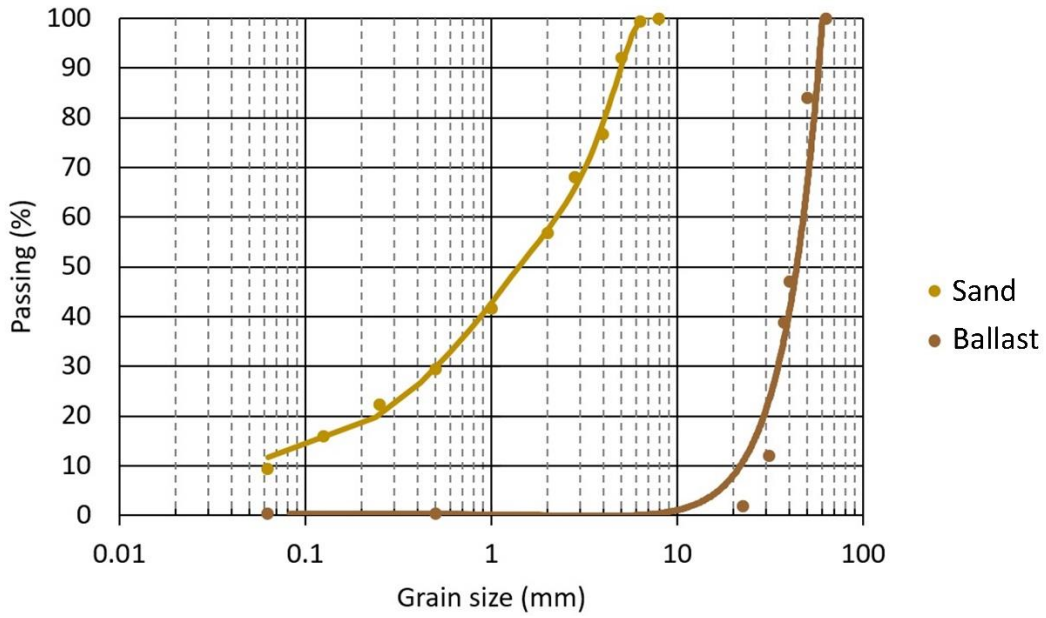

Figure 9: Sieve analysis for sand and ballast.

Specimen preparation and excavation in the full-scale testing facility required the largest amount of time and energy during this study. Overhead cranes and forklifts were employed while handling the 1t bags, sleepers, slabs and other heavy tools. A bobcat excavator and trucks were used during the excavation process. While levelling the slab was easy, as the layer underneath the slab was a highly fluid cementitious mixture, the sleepers in the ballast tests were hard to level due to uneven surface of ballast and this eventually led to some tilt during the testing, whereas in the field the continuous rails help to prevent this rotational movement, although a degree of ballast voiding may still occur.

3 Testing procedure and data acquisition

The same load combinations and durations were implemented in the tests presented in this paper as those used in the experiments carried out by Čebašek et al (2018); this is to allow the reader to directly compare between substructure types. As described by Čebašek et al (2018), redistribution of the axle load was applied over the three-sleeper sections for the static loading case. While half of the axle load was applied on the middle sleeper, one quarter axle load was applied on each neighbouring sleeper. In this way, 100% of the axle load is distributed over the three-sleeper track section during static loading. This approximate redistribution approach was derived from beam-on-elastic-foundation (BOEF) theory. This approach to track deflection analysis replaces the individual sleepers with a continuous support where the load is proportional to the vertical displacement (Powrie, 2016; Connolly, et al., 2020). Young's modulus and 2nd moment of area of rail, and track stiffness are the main parameters considered for the redistribution. The load redistribution, caused by an axle resting on a 3-sleeper section with continuous rail, was implemented using a static loading method (Bian, et al., 2020). For the dynamic loading case, however, each axle load was applied on each sleeper separately without any redistribution. This approach was implemented to both simulate a worst-case scenario and to allow direct comparisons of settlement behaviour between different track types and substructure forms for the same cyclic loading condition. This decision was considered an

important aspect of these particular tests, i.e. to provide a baseline by which performance comparisons could be made and hence future computer models calibrated. In essence, an attempt has been made to standardise the testing programme. **Table 3** shows the details of each considered loading case.

Table 3: Loading sequences of the ballasted and concrete slab track tests.

TEST	Axle load on middle sleeper (kN)	Redistribution of load per actuator (kN)	Redistribution of the load over the sleeper (%)	Frequency (Hz)	Time interval between sleepers (s)	Duration
Static I	63.77	15.94, 31.88, 15.94	25, 50, 25	N/A	N/A	600 s
Static II	83.38	20.84, 41.69, 20.84	25, 50, 25	N/A	N/A	600 s
Dynamic I	117.72	58.86, 58.86, 58.86	100, 100, 100	5.6	0.0065	1.17×10^6 cycles
Dynamic II	166.76	83.38, 83.38, 83.38	100, 100, 100	2.5	0.0065	2.20×10^6 cycles

Two static tests and two cyclic tests were performed. In the static tests, first, a 13-tonne axle load with redistribution was applied on the track for approximately 10 minutes and then the load was increased to simulate a 17-tonne axle load for the same length of time. After these initial tests, cyclic loading began without any load redistribution, by applying a 17-tonne axle load on each sleeper with a time phase lag. The sleepers were therefore subjected to repeated loads to simulate moving axles at 360km/h at a set distance (frequency). Lekarp, et al., (2000) illustrated an element subjected to stress pulses due to a moving wheel load. The vertical and horizontal stress are positive in the soil throughout the passage of the wheel, whereas the shear stress is reversed while the loading is passing by and causing a rotation of the principal stress axes. The principal stress rotation significantly affects the permanent settlement. It is noted that the stationary cyclic loading cannot fully reflect the stress rotation pattern (Bian, et al., 2020). The phased nature of the loading allows for principal stress rotation effects to be simulated.**Figure 10** shows a typical phase/time lag between the sleepers; this phasing mimics the axle moving from one sleeper to the adjacent one in 0.0065 seconds. The cyclic tests were performed at 2 different frequencies: 1.17 million cycles at 5.6Hz and 2.2 million cycles at 2.5Hz. The load applied at 5.6Hz was 58.86kN per actuator, giving 117.72kN per sleeper, and the load at 2.5Hz was 83.38kN per actuator, giving 166.76kN on each sleeper (**Figure 10**).

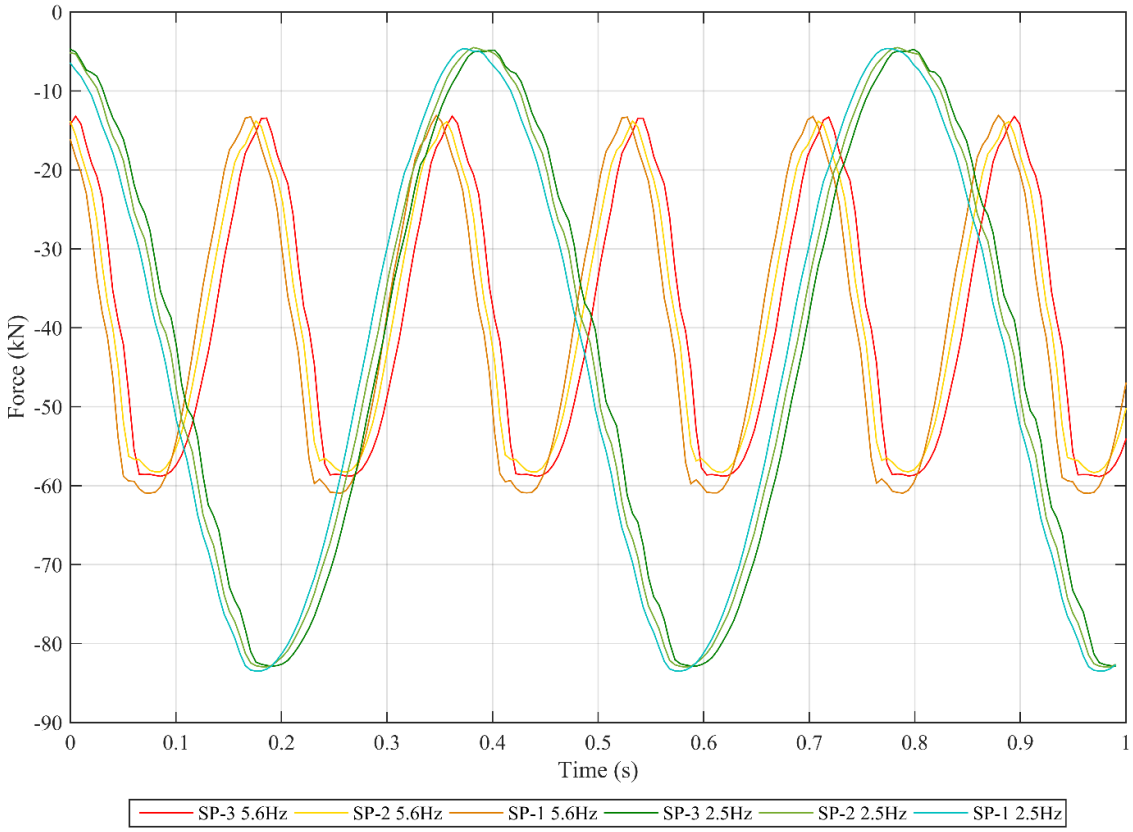

Figure 10: *Time interval of sequential loading of different frequencies in a second*

There were 32 channels actively used to acquire data. The sampling rate of the data acquisition system was 200Hz per channel and each individual item of measuring equipment was connected to a separate channel. Due to the volume of data collected, this paper concentrates on those measurements from the displacement and load cells transducers only. To control the stroke of the actuators, six 300mm long displacement transducers (LVDT) were used.

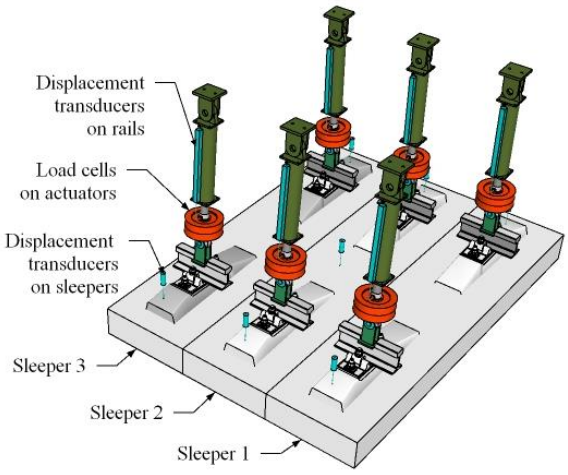

(a)

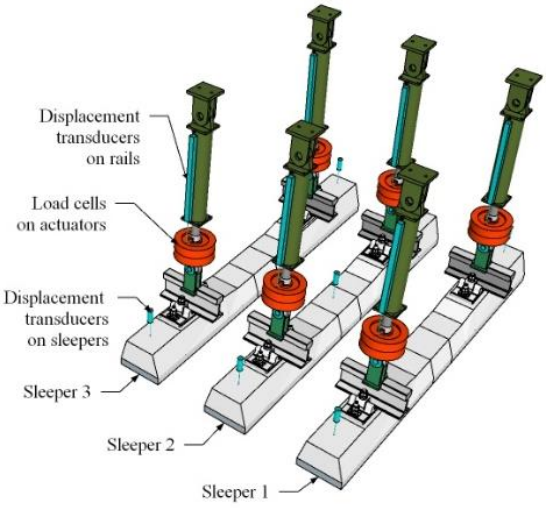

(b)

Figure 11: *LVDT positions and labels (a) slab track (b) ballasted track*

The displacement transducers' locations are represented in **Figure 11**. The LVDT choice was crucial for these tests as both the instantaneous/transient displacement under one cycle, and settlement, which is the permenant deformation under millions of cycles, must be plotted with the same LVDT acquired data. Therefore, they both needed to be sensitive enough to record the sinusoidal motion of the slab, which acquired a hundredth of a millimetre, as well as the accumulated settlement of the sleepers in the ballast after 3.4 million cycles, which was greater than 10 millimetres. The positioning of the LVDTs on the track was set to investigate the elastic deformation of the track as well as the total settlement under accumulated cycles.

4 Analysis

In this section, results related to the static and cyclic tests are presented and analysed.

4.1 Static compressive loading

As mentioned earlier, an initial static distributed axle load was applied on the two tracks. Firstly, 13t (127.54kN) and then 17t (166.76kN) were applied for a duration of approximately 10 minutes each (**Figure 12**). The distribution of these axle loads, over the three-sleeper area, is described in **Table 3**.

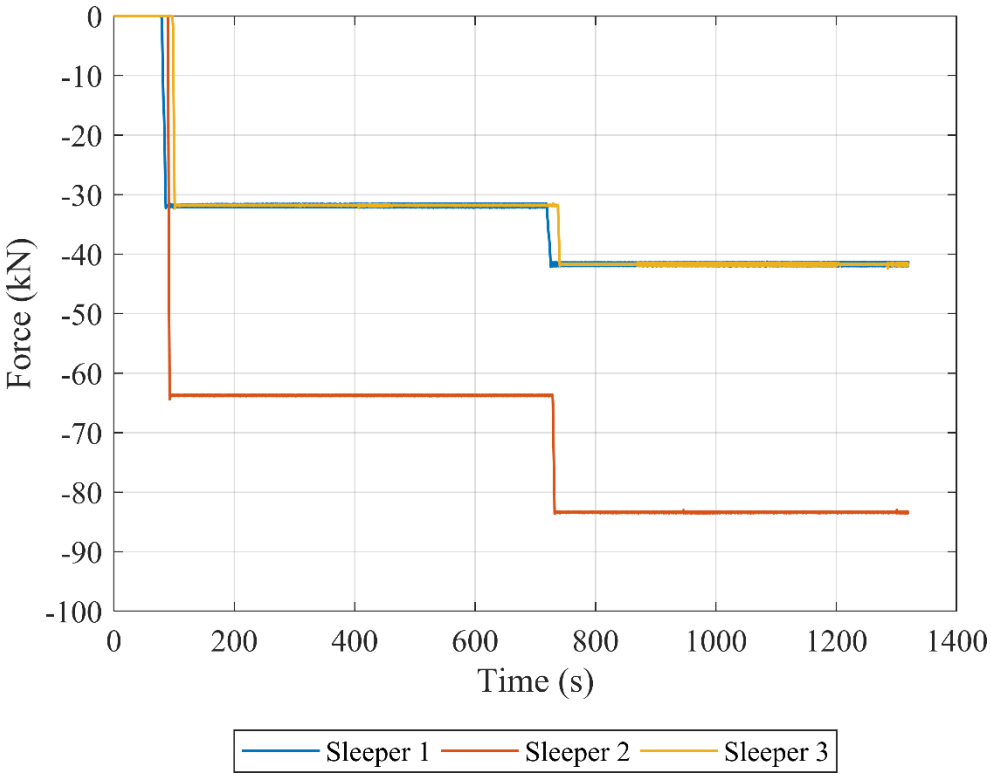

Figure 12: *Distribution of axle loads over three sleepers*

The red line in **Figure 12** represents half of the axle load applied on the middle sleeper (Sleeper 2) while yellow and blue lines represent the quarter of the axle load applied on the adjacent sleepers (Sleeper 1 and Sleeper 3). After completing the static tests, the load was taken off. Since the displacement transducers on the rails and the sleepers show similar results, the average reading of the transducers was used for the analysis. For example, while analysing the displacement of the sleepers, the corner LVDTs (Sleepers 1 and 3) were considered. The average of the relative readings of the transducers at certain times was calculated.

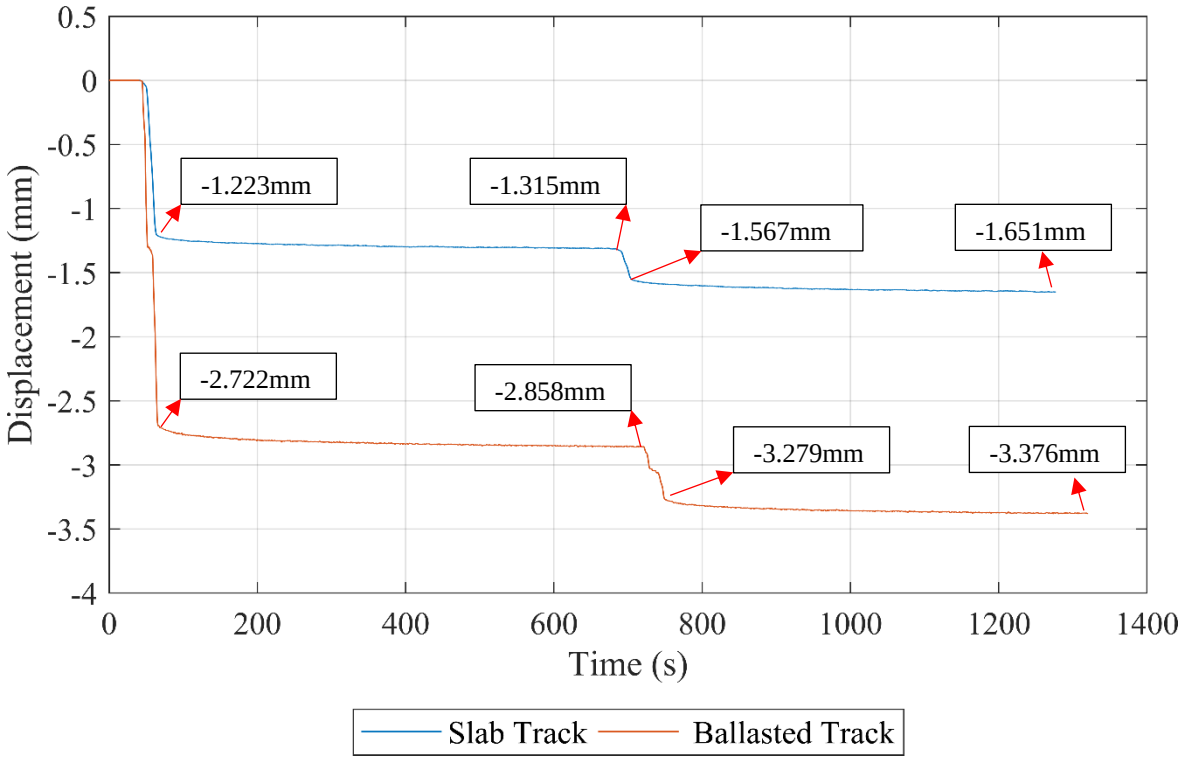

Figure 13: *Average vertical displacement of the rails for concrete slab track and sleepers on ballasted track under static loading*

As can be seen in **Figure 13**, the average displacements of the rails of the slab track are nearly half of those on the ballasted track. The displacement of four rail segments, on the sleepers 1 and 3, was taken into account. It is evident that under the static loading, a large part of the rail displacement is caused by the ballast bed because the same rail pads were used for both types of tracks. The displacement under stationary loading indicates a similar value of rail displacement for ballasted and slab track over the two 10-minute-long loading period, which is around 0.1mm. However, during the static loading when the load increased from 0 to 13t and then from 13t to 17t, the displacement of the rail on ballasted track was nearly double.

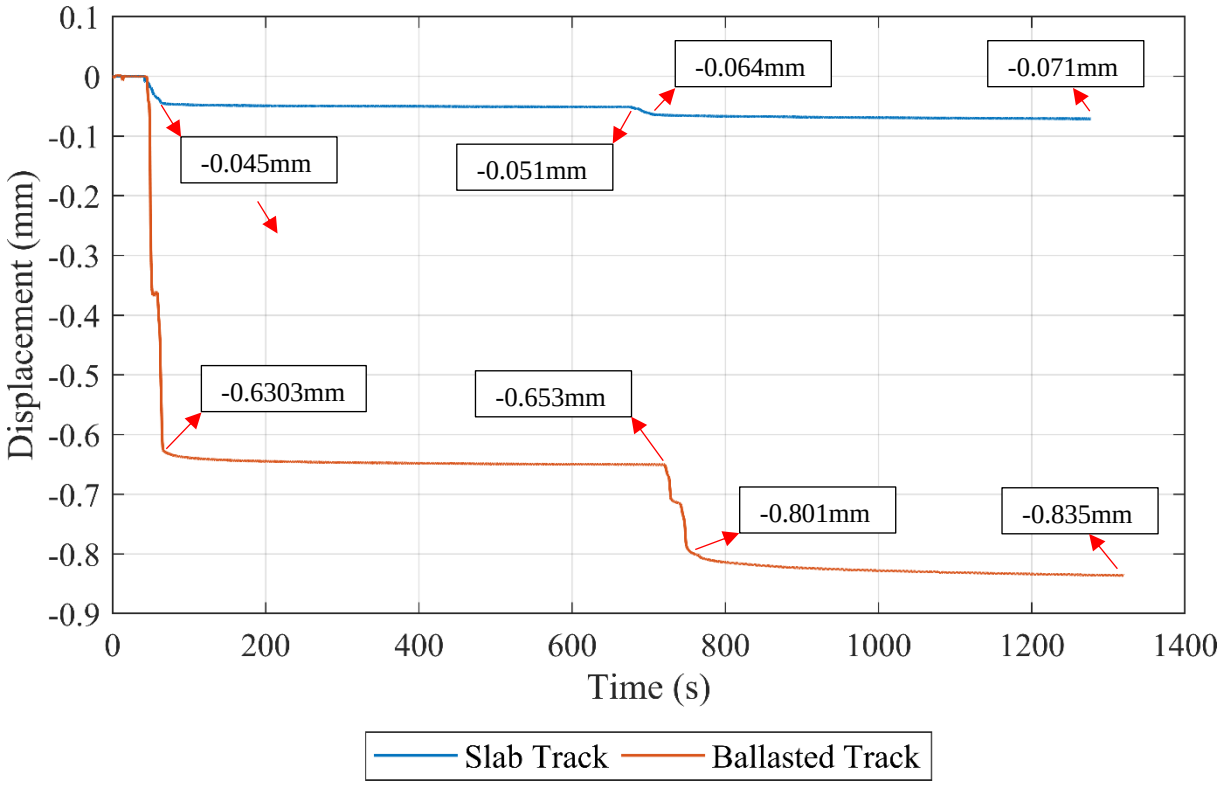

Figure 14: *Vertical displacement of the track on the corners for concrete slab track and sleepers on ballasted track*

Figure 14 shows the displacements on the corners of the concrete slab-track and the ballasted track (Sleeper 1 and Sleeper 3). As expected, the displacements of the sleepers on ballasted track are higher due to the unbound and less stiff nature of the ballast. These displacement values were obtained from the four LVDTs positioned on the surface of the sleepers 1 and 3. The vertical displacement of the ballasted track was more than 10 times the displacement of the slab track when the load was increased from 0 to 13t and then from 13t to 17t. The displacement of the sleepers in the ballasted track during the stationary load was nearly 4 times larger compared to that of the slab track. These results highlight the superior load-distributing properties of the concrete slab-track and hence the reduction of the stress concentrations on the GRS trackbed. The total plastic settlement of the ballasted track after releasing the load was 0.331mm, whereas the slab only settled 0.019mm.

A notable result from the static compression load tests on the concrete slab track was the improved performance of the GRS structure when compared to the ballasted track. In addition to the weight of the HBL, concrete slab and rail segments, 13 tonnes and 17 tonnes of load were applied, and thus, the GRS structure endured firmly. Moreover, the vertical displacement after about 20 minutes of static loading was only 0.07 mm and the total plastic settlement was 0.019mm after removing the load.

4.2 Cyclic loading

In a stable track structure, the magnitude of the axle loads and their accumulation (load cycles) are the main reasons for the permanent vertical track settlement. This plastic settlement, due to *the track tonnage*, leads to changes in the track geometry and hence a deteriorating ride quality.

The transient displacement under individual axles is an important component of the track behaviour. For example, in a ballasted track, if the track stiffness is too low then increased settlement will likely occur, if it is too high then increased rail wear may result. Each layer's individual elastic stiffness modulus contributes to the transient displacement. In conventional ballasted track, vertical stresses reduce relatively quickly with depth compared to the trackbed displacements. In addition to the elastic stiffness modulus of the individual trackbed layers below the ballast, the unbound nature of the ballast itself is another reason for higher displacements of ballasted tracks when compared to a bound system, such as concrete slab track. This is because the elastic stiffness modulus of the unbound ballast is a function of its effective confining pressure as well as other properties such as aggregate angularity and density.

The key parameters leading to the observed settlements and vertical displacements were identified via analysing both total and individual cycles. The cycles were chosen at the beginning and at the end of the tests to determine the stiffness change in the track under high levels of cyclic loading (tonnage). In general, vertical displacement data is represented per second and for two different frequencies of 5.6Hz and 2.5 Hz. The total settlement is also plotted for both frequencies for 1.2 million and 2.2 million cycles, respectively. These points have been chosen so that comparisons to the Čebašek et al. (2018) paper can be directly made.

The mean magnitude of the rail and the sleeper displacements were calculated based on the four LVDTs placed at the sleepers 1 and 3, and in the corners of the slab track. The smoothness of the cycles is directly related to the performance of the data acquisition system; it was found that the LVDTs on the slab and sleepers were more sensitive than the ones on the rails.

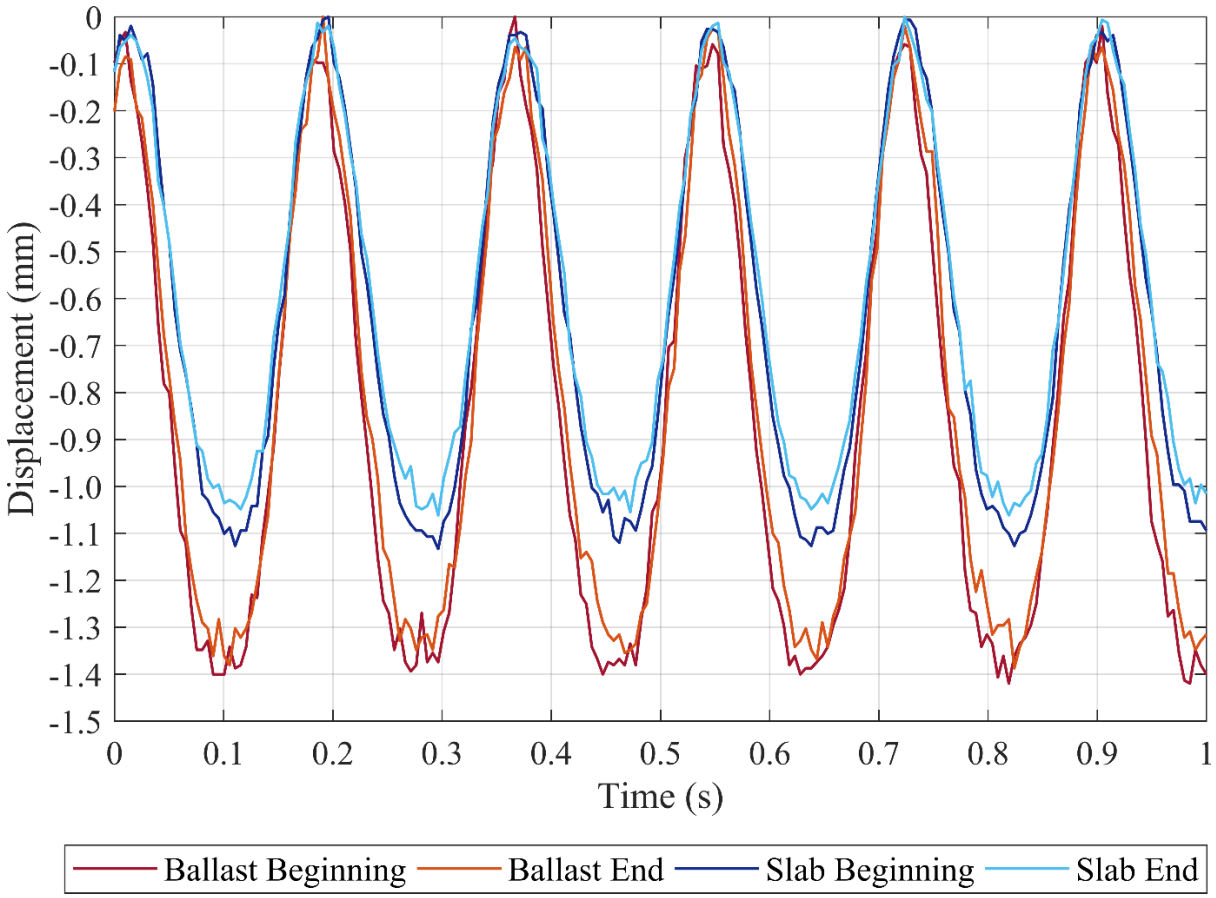

Figure 15: *Average displacement amplitudes of the rails on ballast and concrete slab track at the beginning and the end of the 5.6Hz cycling at 13kN to 58.9kN*

The amplitudes are taken 1000 cycles from the beginning of the tests and 1000 cycles before the end. The average displacement of the rails on the slab at 5.6Hz loading was 1.1mm, whereas it was 1.4mm in the case of the ballasted track (**Figure 15**). The magnitude of the load at this frequency was oscillating between 13kN and 58.9kN. The reduction in the amplitude of the rail displacement was 0.05mm for both tracks.

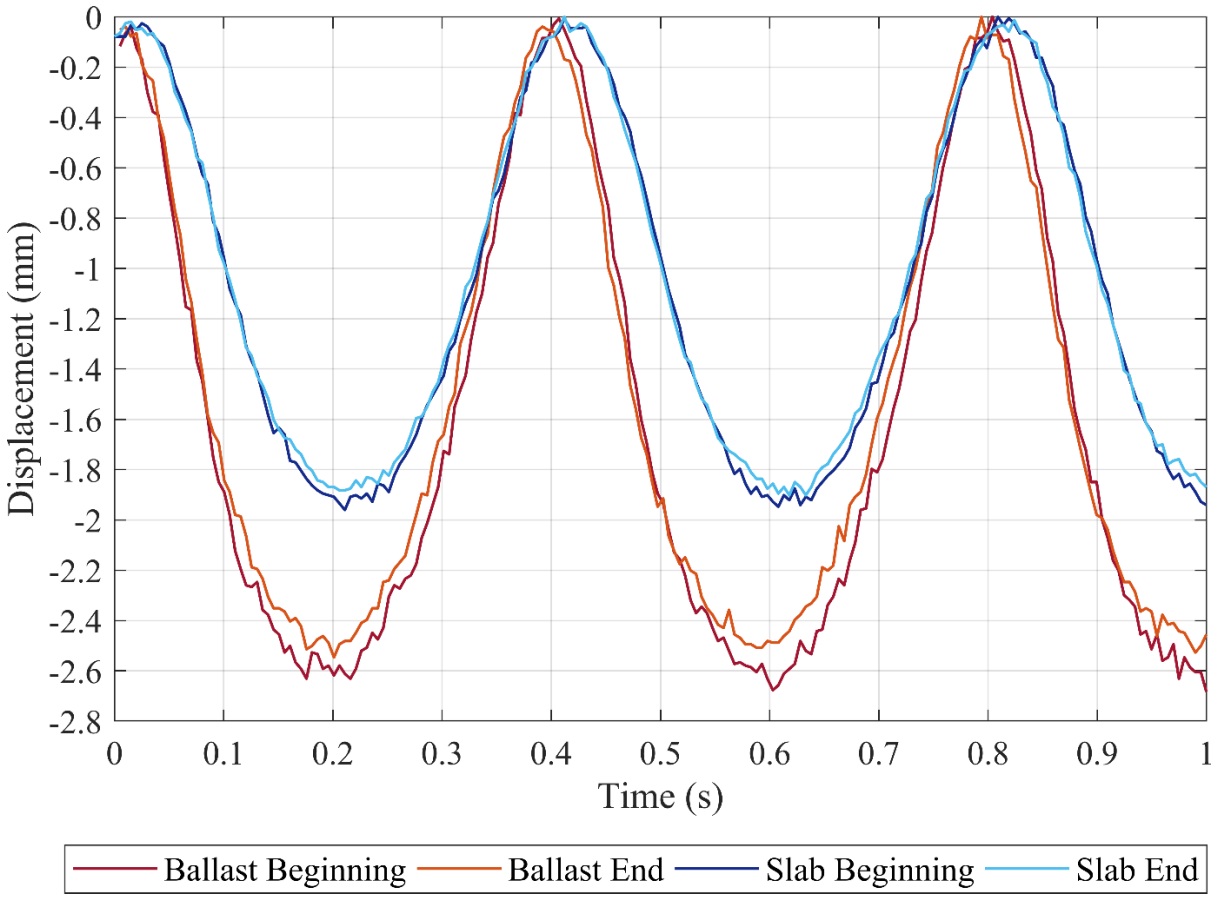

441

442 ***Figure 16:*** *Average displacement amplitudes of the rails on ballast and concrete slab track at the*
443 *beginning and the end of the 2.5Hz cycling at 5kN and 83.4kN*

444 In **Figure 16** the mean displacements of the rails on both tracks are presented. The rail on the
445 slab deflected around 1.9mm, whereas in the ballasted track case it deflected 2.6mm under
446 83.4kN cyclic loading (as mentioned above this equates to a phased 17t axle load on individual
447 sleepers without redistribution). The reduction in amplitude in the slab's rail displacement was
448 much smaller than that on the ballasted track.

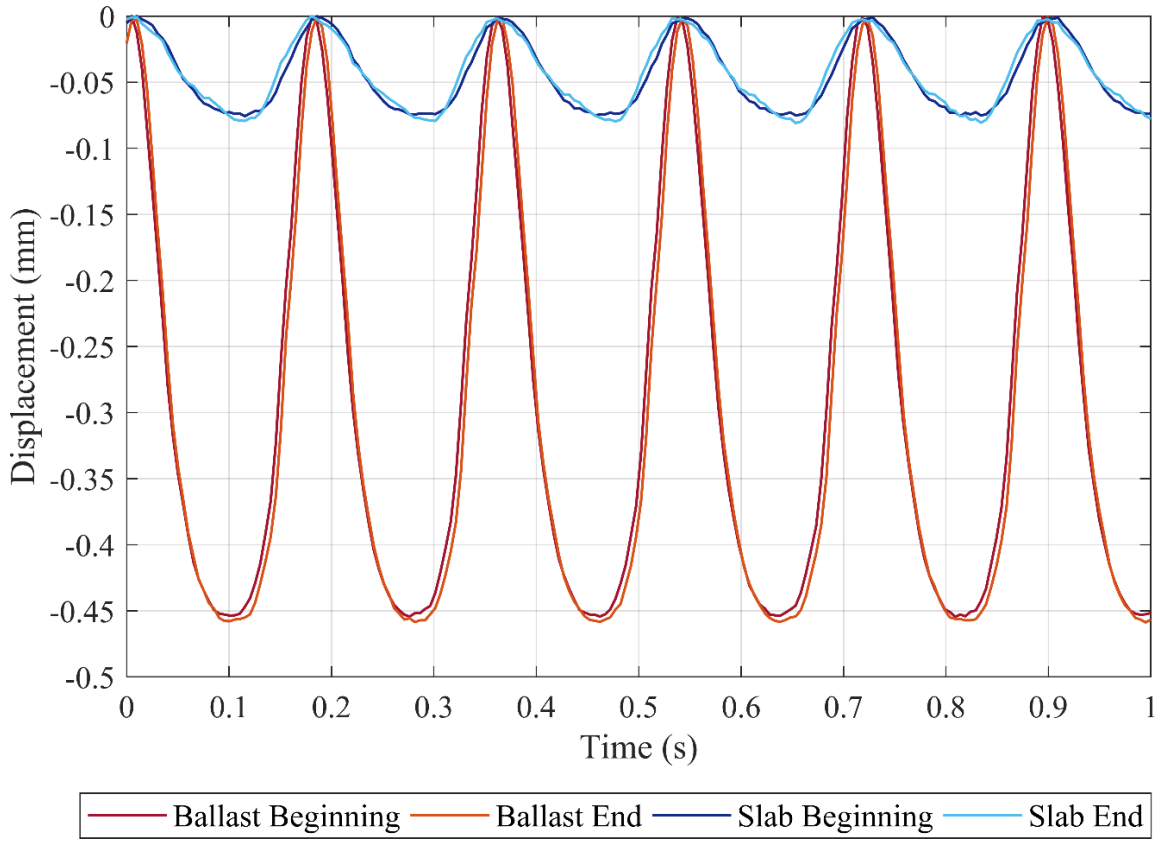

Figure 17: *Average displacement amplitudes of the sleepers of ballast and concrete slab track at the beginning and the end of the 5.6Hz cycling at 13kN to 58.9kN*

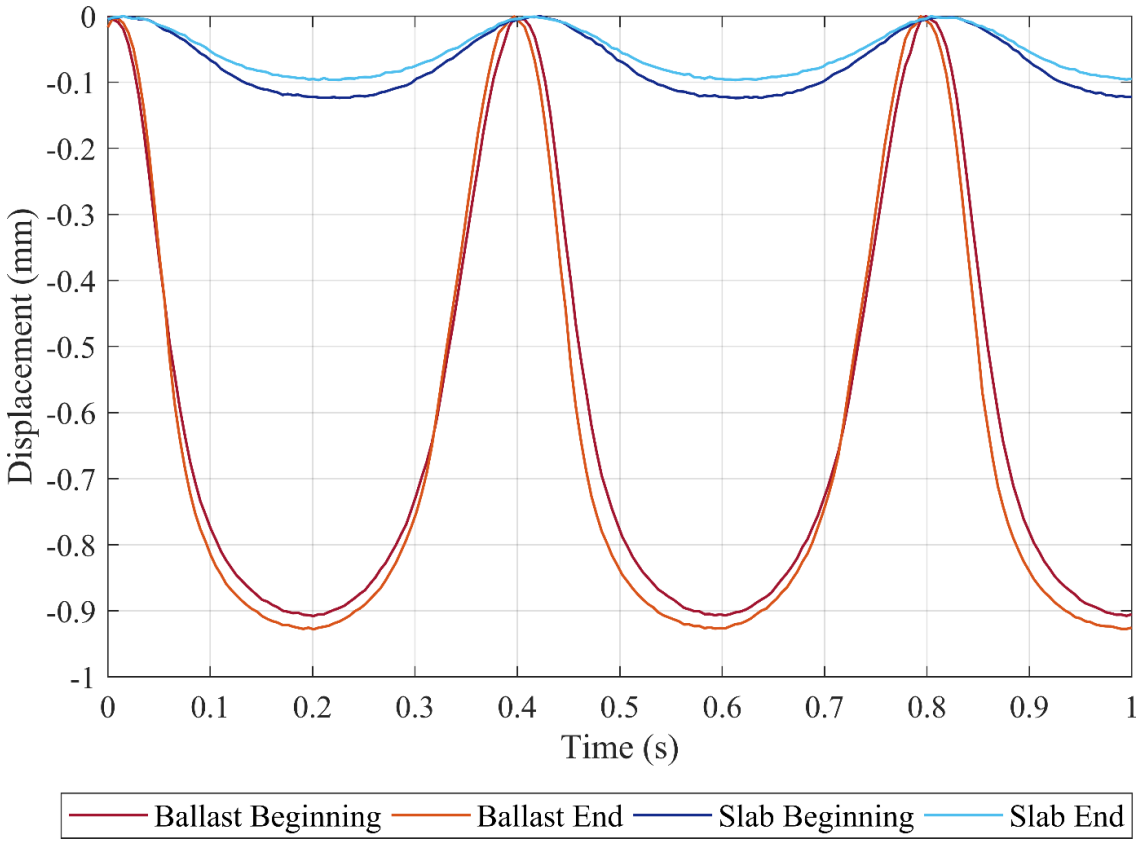

Figure 18*: Average displacement amplitudes of the sleepers of ballast and concrete slab track at the beginning and the end of the 2.5Hz cycling at 5kN and 83.4kN*

Figure 17 and **Figure 18** indicate the mean displacements of the sleepers in the ballasted track and the slab under 5.6Hz and 2.5Hz loading. Contrary to the elastic behaviour of the slab, ballast performed in a more complex manner due to its unbound and non-linear nature. While thetransient displacement of the slab was quite uniform according to the LVDTs on the slab, the displacement of the sleepers in the ballast varies significantly among the LVDTs. The average overall displacement of the LVDTs at the end of each loading phase was slightly greater than the average overall displacement of the LVDTs at the start of the loading. This was traced to one LVDT which exhibited a slight inconsistency in readings between the beginning and final displacements for the ballasted track. This LVDT recorded a 0.13mm increase in displacement over 2.2 million load cycles, whereas all the other LVDTs generally showed a slight reduction in the amplitude (as would be expected). This increase in displacement is, however, very small (a fraction of a mm) compared to the full amplitude of each sleeper displacement. It is conceivable that this may indicate a small movement of the anchoring system near this particular LVDT, but could also simply be within experimental error of the measurement system for this particular LVDT over the 2.2 million load cycles. Even so, the average of the LVDTs was presented for the consistency in the representation. These LVDTs were placed on the surface of the slab and the sleepers.

The mean displacement of the slab under a single cycle at 5.6Hz loading was 0.079mm and 0.111mm at 2.5Hz, which corresponded to load increase from 58.9kN to 83.4kN, respectively. The displacement of the sleepers in the ballasted track was 0.45mm throughout the 5.6Hz loading. It was 0.9mm when the frequency decreased to 2.5Hz because the load increased from 58.9kN to 83.4kN, as mentioned above.

Overall, the rail displacement is directly linked to the displacement of the wheels and is always higher than the sleeper displacement due to the presence of the railpads. The displacements of both rail and sleeper are recorded during the testing for future analysis of the railpads efficiency in reducing the transmitted displacement.

4.3 Permanent Settlement

In **Figure 19**, the average cumulative settlement of the slab and ballasted tracks are presented.

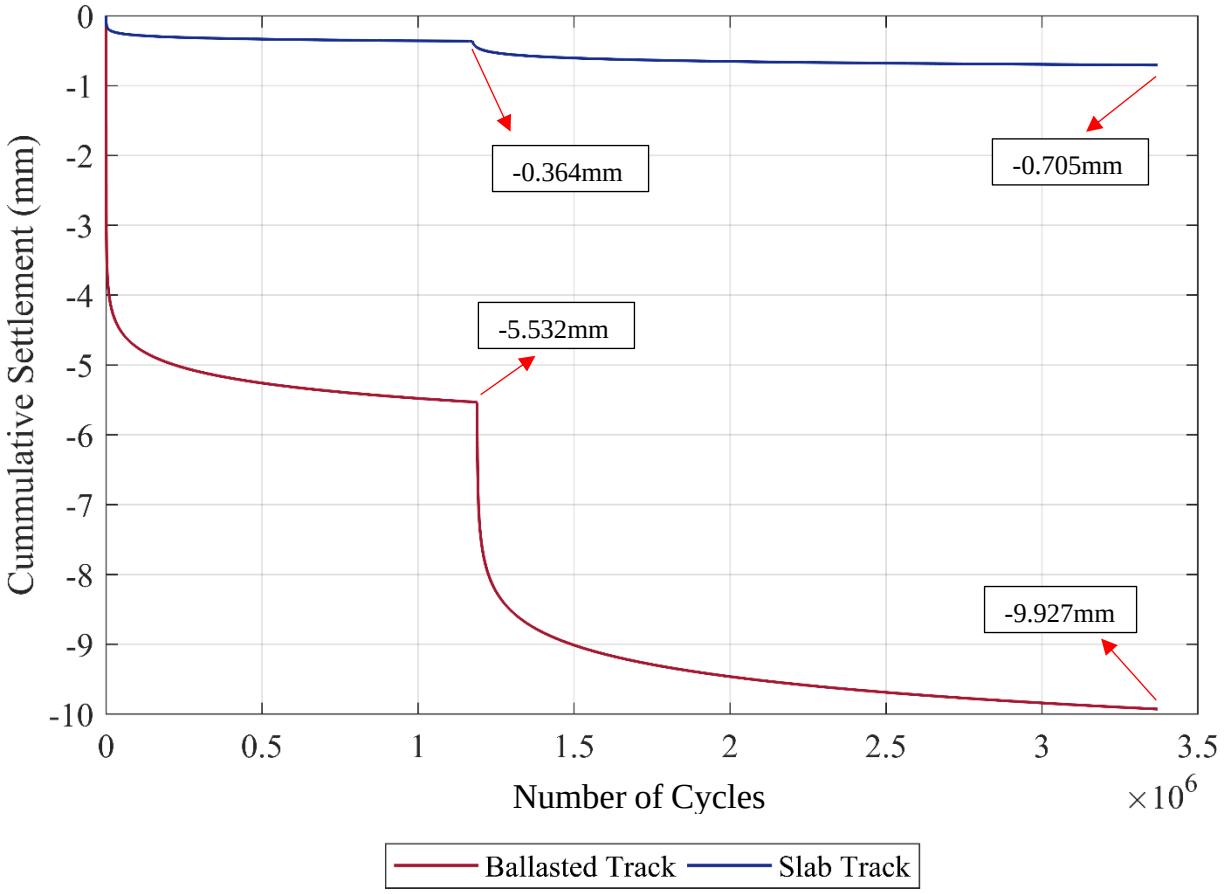

Figure 19: *Cumulative settlement of slab and ballasted track at each frequency vs the number of cycles*

The blue curve shows the settlement values at the corners of the concrete slab track. The average cumulative settlement of the concrete slab track is 0.705mm under two consecutive stages of cyclic loading. The average settlement for the first loading phase (5.6 Hz for 1.2 million cycles) is 0.364mm, whereas the rest of the cumulative settlement is generated by the second phase of loading (2.5Hz for 2.2 million cycles). The red curve shows the settlement values at the end of the sleepers 1 and 3 in the ballasted track. The average cumulative settlement at 5.6Hz for 1.2 million cycles was 5.532mm, whereas the rest of the cumulative settlement is generated by the second phase of loading (2.5Hz for 2.2 million cycles) and reaches 9.927mm.

As with other track tests reported in the literature, significant parts of the plastic deformation are generated by the initial load cycles. After this initial phase, the settlement follows a reduced downward trend in the ballasted track. In the concrete slab track tests, the track shows a much-reduced settlement curve after the initial cycles compared to that of the ballasted track (i.e. it starts to level off very quickly).

5 Conclusion

A geosynthetically reinforced soil with retaining wall (GRS-RW) was tested at full-scale as an alternative to a conventional rail embankment. The soil fill (subgrade) was formed of two layers

at different stiffnesses and were compacted to high-speed rail standards. The soil stiffness parameters were measured using *in-situ* soil testing techniques and the soil was reinforced using uniaxial geogrids wrapped around granular bags. These bags provide lateral confinement during placement and compaction of the fill materials.

A three-sleeper section of a concrete slab track and a ballasted track were placed on the GRS structure alternately. The loads were applied using six individual actuators connected to the track superstructure via a rail connector. Firstly, two different static loads were applied with redistribution over the track structure to account for the bending stiffness of a rail section. Then two different cyclic loading frequencies were applied in a phased manner to mimic a train moving at 360km/h. For the cyclic loading case, no load distribution was applied to allow direct comparisons with earlier published work and to represent a worst-case scenario. The results are summarized as follows:

1- The GRS-RW structure showed good performance under both static and cyclic loading comparing to the experiments carried out by Čebašek, et al. (2018), despite the fact the structure was confined on the two lateral sides and the other two were free walls anchored into the fill.
2- For each track, more than 3.3 million load cycles were applied. The ballasted track presented a large settlement compared to the slab track, which was approximately 15 times greater in both types of cyclic loading. The magnitude of the plastic strain increment for the cyclic loops at the end and beginning of the loading was only slightly different indicating that the stiffness and density of the substructure had not increased significantly during shakedown.
3- The amplitude of the rail displacement under individual cycles at 5.6 Hz and 2.5 Hz loading was approximately 25% lower for the slab track when compared to the case of ballasted track. The major part of the elastic displacement of the rail was caused by the railpad which was about 93% for the rail on the slab track and 66% on the ballasted track.
4- The amplitude of the sleeper displacement on the ballasted track was approximately 6 to 7 times greater than the amplitude of the slab under individual cyclic loading, demonstrating that the vertical and bending track stiffnesses of the slab are much higher than those of the ballasted track, even for a reduced track length.

To conclude, the transient displacement and permanent settlement for the case of slab track were significantly lower than those of the ballasted track. Hence, the superior performance of the slab track, which may require less maintenance and thus lead to increased traffic availability. The enhanced inherent quality of the slab track in terms of stability and durability is likely to ensure a smooth ride quality and lower life-cycle costs.

Acknowledgements

The authors are grateful to the Engineering and Physical Sciences Research Council (EPSRC) for funding this work under Grant Numbers EP/N009207/1 and EP/N009215/1. Tensar and Max-Bögl are also acknowledged for their support with regards to the experimental testing stages.

6 References

Abadi, T., L. Le Pen, A. Zervos, and W. Powrie. 2016. "A review and evaluation of ballast settlement models using results from the Southampton Railway Testing Facility (SRTF)." *Procedia engineering* 143: 999-1006.

Alva-Hurtado, J., and E. Selig. 1981. "Permanent strain behavior of railroad ballast." *Proceedings of the International Conference on Soil Mechanics and Foundation Engineering* 1: 543-546.

Berg, R.R., B.R. Christopher, and N.C. Samtani. 2009. *Design of Mechanically Stabilized Earth Walls and Reinforced Soil Slopes-Volume II. Report No. FHWA-NHI-10-025.* Washington, D.C: National Highway Institute, Federal Highway Administration.

Bian, X., H. Jiang, C. Cheng, Y. Chen, R. Chen, and J. Jiang. 2014. "Full-scale model testing on a ballastless high-speed railway under simulated train moving loads." *Soil Dynamics and Earthquake Engineering* 66: 368-384.

Bian, X., Li, W., Qian, Y. and Tutumluer, E., 2020. Analysing the effect of principal stress rotation on railway track settlement by discrete element method. *Géotechnique*, 70 (9), pp.803-821.

Brown, S., B. Brodrick, N. Thom, and G. McDowell. 2007. "The Nottingham railway test facility, UK." *Proceedings of the Institution of Civil Engineers-Transport* 160 (2): 59-65.

Čebašek, T. M., A. F. Esen, P. K. Woodward, O. Laghrouche, and D. P. Connolly. 2018. "Full scale laboratory testing of ballast and concrete slab tracks under phased cyclic loading." *Transportation Geotechnics* 17: 33-40.

Connolly, D.P., Dong, K., Alves Costa, P., Soares, P. and Woodward, P.K., 2020. High speed railway ground dynamics: a multi-model analysis. *International Journal of Rail Transportation*, pp.1-23.

Connolly, D., A. Giannopoulos, and M.C. Forde. 2013. "Numerical modelling of ground borne vibrations from high speed rail lines on embankments." *Soil Dynamics and Earthquake Engineering* 46: 13-19.

Connolly, D.P., G. Kouroussis, P.K. Woodward, P.A. Costa, O. Verlinden, and M.C., Forde. 2014. "Field testing and analysis of high speed rail vibrations." *Soil Dynamics and Earthquake Engineering, 67* 102-118.

Dahlberg, T. 2001. "Some railroad settlement models—a critical review." *Proceedings of the Institution of Mechanical Engineers, Part F: Journal of Rail and Rapid Transit* 215 (4): 289-300.

Dong, K., D.P. Connolly, O. Laghrouche, P.K. Woodward, and P.A. Costa. 2018. "The stiffening of soft soils on railway lines." *Transportation Geotechnics* 17: 178-191.

576 Helwany, S. M. B., J. T.H. Wub, and B. Froessl. 2003. "GRS bridge abutments—an effective
577 means to alleviate bridge approach settlement." *Geotextiles and Geomembranes* 177-
578 196.

579 Herold, A. 2005. "Brückenwiderlager aus KBE-Kunststoffbewehrte Erde, Einsatzgebiete Und
580 Anwendungsgrenzen." *Geotechnik-Kolloquium, Freiberg, Technische Institut für*
581 *Geotechnik der Universität Bergakademie Freiberg, Heft* (Geotechnik-Kolloquium,
582 Freiberg, Technische Institut) 195-217.

583 Horii, K., H. Kishida, M. Tateyama, and F. Tatsuoka. 1994. "Computerized design method for
584 geosynthetic-reinforced soil retaining walls for railway embankments." R*ecent Case*
585 *Histories of Permanent Geosynthetic-Reinforced Soil Retaining Walls* 205-218.

586 Indraratna, B., N. T. Ngo, and C. Rujikiatkamjorn. 2012. "Deformation of coal fouled ballast
587 stabilized with geogrid under cyclic load." *Journal of Geotechnical and*
588 *Geoenvironmental Engineering* 139 (8): 1275-1289.

589 Kim, D.S., and U.J. Kim. 2016. "Performance Evaluation of a New Type of Abutment with
590 Geosynthetics." *Proceedings of the Third International Conference on Railway*
591 *Technology: Research, Development and.* Stirlingshire, Scotland: Civil-Comp Press.
592 33.

593 Koseki, J. 2012. "Use of Geosynthetics to Improve Seismic Performance of Earth Structures."
594 *Geotextiles and Geomembranes* (http://www.mercerlecture.com/) 34: 51-68.
595 http://www.mercerlecture.com/.

596 Koseki, J., R. J. Bathurst, E. Güler, J. Kuwano, and M. Maugeri. 2006. "Seismic stability of
597 reinforced soil walls." *Invited keynote paper, 8th International Conference of*
598 *Geosynthetics, Yokohama* 18-22.

599 Koseki, J., Y. Munaf, F. Tatsuoka, M. Tateyama, K. Kojima, and T. Sato. 1996. "Shaking and
600 tilt table tests of geosynthetic-reinforced soil and conventional-type retaining walls."
601 *Geosynthetics international* 73-96.

602 Lee, K.Z.Z., and J. T.H. Wu. 2004. "A synthesis of case histories on GRS bridge supporting
603 structures with flexible facing." *Geotextiles and Geomembranes* 181-204.

604 Lekarp, F., Isacsson, U. and Dawson, A., 2000. State of the art. I: Resilient response of unbound
605 aggregates. *Journal of transportation engineering*, 126 (1), pp.66-75.

606 Lenart, S., M. Kralj, S.P. Medved, and J. Šuler. 2016. "Design and construction of the first
607 GRS integrated bridge with FHR facings in Europe." *Transportation Geotechnics 8* 26-
608 34.

609 Powrie, W. ed., 2016. A Guide to Track Stiffness: August 2016. University of Southampton
610 Department of Civil & Enviromental Engineering.

611 Punetha, P., S. Nimbalkar, and H. Khabbaz. 2020. "Evaluation of additional confinement for
612 three-dimensional geoinclusions under general stress state." *Canadian Geotechnical*
613 *Journal* 57 (3): 453-461.

614 Sato, Y. 1995. "Japanese studies on deterioration of ballasted track." *Vehicle system dynamics*
615 24 (1): 197-208.

616 Selig, E. T., and J. M. Waters. 1994. *Track geotechnology and substructure management.*
617 Thomas Telford.

618 Shenton, M. 1985. "Ballast deformation and track deterioration." *Track technology* 253-265.

619 Singh, RP, S. Nimbalkar, S. Singh, and D. Choudhury. 2020. "Field assessment of railway
620 ballast degradation and mitigation using geotextile." *Geotextiles and Geomembranes*
621 48 (3): 275-283.

622 Skinner, G. D., and R. K. Rowe. 2005. "Design behaviour of geosynthetic reinforced retaining
623 wall and bridge abutment on yielding foundation." *Geotextiles and Geomembranes*
624 234-260.

625 Tatsuoka, F., and K. Watanabe. 2015. "Design, Construction, and Performance of GRS
626 Structures for Railways in Japan." In *Ground Improvement Case Histories.*
627 *Compaction, Grouting and*, 657-692. Elsevier.

628 Tatsuoka, F., M. Tateyama, J. Koseki, and T. Yonezawa. 2014. "Geosynthetic-Reinforced Soil
629 Structures for Railways in Japan." *Transp. Infrastruct. Geotech* 3–53.

630 Tatsuoka, F., M. Tateyama, T. Uchimura, and J. Koseki. 1997. "Geosynthetic-reinforced soil
631 retaining walls as important permanent structures Geosynthetics international."
632 *Geosynthetics international, Vol. 4, No. 2* 81-135.

633 Tatsuoka, F., M. Tateyama, Y. Mohri, and K. Matsushima. 2007. "Remedial treatment of soil
634 structures using geosynthetic-reinforcing technology." *Geotextiles and Geomembranes*
635 204–220.

636 Tatsuoka, F. 2019. "Geosynthetic-reinforced soil structures for transportation: from walls to
637 bridges." *Australia New Zealand Conference on Geomechanics, 13th, 2019, Perth,*
638 *Western Australia.* Australia.

639 Thom, N., and J. Oakley. 2006. "Predicting differential settlement in a railway trackbed."
640 *Proceedings of Railway foundations conference: Railfound* 6: 190-200.

641 Woodward, P., J. Kennedy, O. Laghrouche, D. Connolly, and G. Medero. 2014. "Study of
642 railway track stiffness modification by polyurethane reinforcement of the ballast."
643 *Transportation Geotechnics* 1 (4): 214-224.

644 Wu, Jonathan T.H. 2018. *Geosynthetic Reinforced Soil (GRS) Walls.* John Wiley & Sons.

Yonezawa, T., T. Yamazaki, M. Tateyama, and F. Tatsuoka. 2014. "Design and construction of geosynthetic-reinforced soil structures for Hokkaido high-speed train line." *Transportation Geotechnics* 3-20.

Yu, Z., D. P. Connolly, P. K. Woodward, and O. Laghrouche. 2019. "Settlement behaviour of hybrid asphalt-ballast railway tracks." *Construction and Building Materials* 208: 808-817.

Yu, Z., P.K. Woodward, O. Laghrouche, and D.P., Connolly. 2019. "True triaxial testing of geogrid for high speed railways." *Transportation Geotechnics* 100247.